Journal Pre-proof

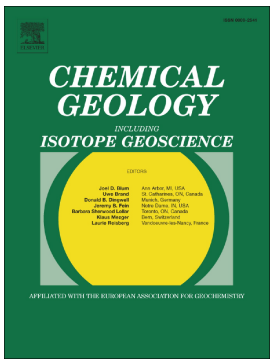

Enrichment of heavy calcium isotopes in saprolite due to secondary mineral formation

Utpalendu Haldar, Ramananda Chakrabarti, Roberta L. Rudnick

PII: S0009-2541(23)00366-2

DOI: https://doi.org/10.1016/j.chemgeo.2023.121666

Reference: CHEMGE 121666

To appear in: *Chemical Geology*

Received date: 15 December 2022

Revised date: 28 July 2023

Accepted date: 8 August 2023

Please cite this article as: U. Haldar, R. Chakrabarti and R.L. Rudnick, Enrichment of heavy calcium isotopes in saprolite due to secondary mineral formation, *Chemical Geology* (2023), https://doi.org/10.1016/j.chemgeo.2023.121666

Enrichment of heavy calcium isotopes in saprolite due to secondary mineral formation

Utpalendu Haldar[1], Ramananda Chakrabarti[1*], Roberta L. Rudnick[2]

1. Centre for Earth Sciences, Indian Institute of Science, Bangalore 560012, India.
2. Department of Earth Science and Earth Research Institute, University of California, Santa Barbara, CA 93106, USA

*Corresponding Author (ramananda@iisc.ac.in/ramananda@gmail.com)

Abstract

Calcium stable isotopes were analyzed in well-characterized saprolite developed on a Mesozoic metadiabase dike near Cayce, South Carolina, to determine the degree and sense of isotopic fractionation during chemical weathering. The $\delta^{44/40}$Ca values (relative to NIST SRM 915a) of the saprolites, measured using double-spike TIMS, vary significantly (0.91‰ to 1.26‰), and are generally higher than the $\delta^{44/40}$Ca value of the unweathered metadiabase (0.98‰), which overlaps, within analytical uncertainties, $\delta^{44/40}$Ca estimates of the bulk silicate Earth. The $\delta^{44/40}$Ca values of the saprolites negatively correlate with bulk density, and Ti-normalized calcium concentrations, and positively correlate with chemical index of alteration (CIA) values. These trends reflect loss of light Ca isotopes to the hydrosphere during metadiabase weathering. Using insoluble incompatible elements ratios (e.g., Th/Nb) we estimate that the influence of aeolian dust is minimal (3% - 11%) and therefore unable to explain the observed variation in Ca isotope composition. Selective weathering of rock-forming minerals like plagioclase and clinopyroxene cannot explain the high $\delta^{44/40}$Ca values (> 1 ‰) of the saprolites based on mass balance constraints. Samples with higher kaolinite/smectite ratio have higher $\delta^{44/40}$Ca values and lower concentrations of Ca, which suggests the loss of Ca from smectite-rich clays during progressive weathering. In this case, the lighter isotopes are preferentially lost, leaving the residual clays enriched in heavier isotopes of Ca. The $\delta^{44/40}$Ca values of saprolites correlate positively with δ^{26}Mg and negatively with δ^{7}Li values of the same samples, which further suggests that Ca stable isotopic variability of the Cayce metadiabase saprolites is controlled by formation of clay minerals and progressive loss of Ca during saprolitization. The enrichment of heavy Ca isotopes in saprolites with progressive loss of Ca can be modeled using Rayleigh distillation, with apparent fractionation factors between saprolites and fluid (α) of 1.00005 to 1.00015.

Keywords

Metadiabase, Saprolite, Chemical weathering, Calcium isotopes, Clay minerals.

1. Introduction

Chemical weathering involves mineral dissolution and secondary mineral formation (e.g., clays, carbonates, oxides, and hydroxides). It influences the composition of the atmosphere, hydrosphere, and continental crust. Silicate weathering releases soluble elements such as Ca, which then precipitates in marine carbonates thereby sequestering CO_2 (1 mole of CO_2 for every mole of Ca) and controlling atmospheric CO_2 concentration over geological timescales (Urey, 1952). During chemical weathering, mobile elements are preferentially leached out of rocks into the hydrosphere causing the relative concentration of immobile elements to increase in the weathered regolith. This modifies the composition of the bulk continental crust (Lee et al., 2008; Liu and Rudnick, 2011) and impedes estimating the concentrations of soluble elements and their isotopes in the upper continental crust, as such estimates are often based on weathered products such as shales, loess, and glacial diamictites (e.g., Chauvel et al., 2014; Gaschnig et al., 2016; Nan et al., 2018; Teng et al., 2004). The chemical and isotopic changes that accompany chemical weathering can be quantified by studying weathering profiles. Such studies are particularly important in understanding the influence of chemical weathering on the stable isotope systematics of soluble elements in the surface environment (e.g., H, Li, O, Mg, K, Ca, Ba).

Previous work on weathering profiles has shown that stable isotopes of the alkali elements Li and K strongly fractionate during chemical weathering, with the heavier isotope partitioning preferentially into water, leaving an isotopically light regolith (e.g., Pistiner and Henderson, 2003; Kisakurek et al., 2004; Rudnick et al., 2004; Teng et al., 2020). Isotopes of the alkaline earth element Mg are also strongly fractionated during chemical weathering; however, the direction of fractionation is the opposite of Li and K, with the weathered residue enriched in the heavier isotopes compared to water (Teng et al., 2010a; Liu et al., 2014). By contrast, isotopes of Ba, also an alkaline earth element, appear to fractionate like Li and K – with the regolith becoming isotopically lighter (Gong et al., 2019). These studies have shown that isotopic fractionation is controlled by the relative strengths of the bonds formed by the element of interest in the two substances (e.g., water vs. secondary minerals in the regolith), with heavier isotopes preferentially entering sites having stronger bonds. Bond strength, in turn, is determined by the coordination number of the site, with stronger bonds occurring in sites having lower coordination numbers.

Calcium is the most abundant alkaline earth metal in Earth's crust and is soluble during chemical weathering. It has six stable isotopes: ^{40}Ca (96.941%), ^{42}Ca (0.657%), ^{43}Ca (0.135%), ^{44}Ca (2.086%), ^{46}Ca (0.004%) and ^{48}Ca (0.187%); the relative mass difference ($\Delta m/m$=20%) between the heaviest and lightest isotopes of calcium is high, which makes Ca isotopes prone to mass-dependent fractionation. Stable isotopic fractionation of Ca isotopes is reported using the standard δ (delta) notation relative to different standards like NIST SRM 915a, 915b (both carbonates), modern seawater, and the estimated value of the bulk silicate Earth (BSE) (e.g., Chakrabarti et al., 2021).

Terrestrial igneous rocks and their constituent minerals display ~2.5 ‰ variability in $\delta^{44/40}$Ca values while even larger variability is observed in metamorphic rocks and their minerals (e.g., Antonelli and Simon, 2020). This variability is due to the differing bonding environments within minerals, magmatic and metamorphic processes and associated kinetic effects (e.g., growth rate of crystals, hydrothermal mineral precipitation, mantle metasomatism, high temperature metamorphism in lower crust) and mixing of isotopically distinct reservoirs (e.g., Antonelli and Simon, 2020; Banerjee et al., 2021). While the $\delta^{44/40}$Ca value of the BSE, relative to SRM 915a, is estimated to be 0.84 ± 0.05 ‰ (Kang et al., 2017), modern oceans have a very high $\delta^{44/40}$Ca value of ~1.92 ‰ (relative to SRM 915a) (e.g., Fantle and Tipper, 2014). Such isotopically heavy sea water is explained by the preferential removal of the lighter isotopes of Ca during precipitation of inorganic and biogenic marine carbonates (e.g., Farkas et al., 2007; Blättler et al., 2015). Although the $\delta^{44/40}$Ca values of the dissolved load of major global rivers are highly variable (0.20-1.70 ‰), ~95% of the $\delta^{44/40}$Ca values in the dissolved load fall within the range 0.31-1.41 ‰, with a mean $\delta^{44/40}$Ca value of 0.86 ‰ (n = 259), which is estimated to be the global riverine flux to the modern oceans (Tipper et al., 2006; Fantle and Tipper, 2014). The large range in $\delta^{44/40}$Ca values of the dissolved load of rivers reflects the distinct compositions of watersheds as well as the complexity of chemical weathering processes (e.g., Tipper et al., 2006; Fantle and Tipper, 2014; Jacobson et al., 2015). Studies of chemical weathering have shown that the formation of secondary minerals, plant uptake, and clay formation can lead to fractionation of Ca isotopes (e.g., Tipper et al., 2006; Fantle et al., 2012; Nelson et al., 2021; Chen et al., 2023) but young soils in a proglacial weathering environment show $\delta^{44/40}$Ca values that are indistinguishable from the rocks from which they were derived (Hindshaw et al., 2011). To date, studies on weathering profiles are lacking for Ca isotopes.

Selective weathering of rock-forming silicate minerals, which have unique Ca isotopic compositions due to differences in bonding environments, can introduce variability in $\delta^{44/40}$Ca in weathered samples (up to 0.42 ‰, Banerjee and Chakrabarti, 2018). Additionally, experimental studies of exchange and adsorption of Ca onto clays found within the continental regolith show that such processes may fractionate Ca isotopes. However, these experimental studies have yielded contrasting results; Ockert et al. (2013) found that illite and kaolinite adsorb the lighter isotopes of calcium on their surfaces, whereas other experiments do not show any significant Ca isotope fractionation during desorption or adsorption on kaolinite, while montmorillonite preferentially adsorbs lighter isotopes of calcium (Brazier et al., 2019). These contrasting results could reflect the mineralogical (e.g., nature of clay mineral) and structural control (exchangeable surface Ca versus non-exchangeable fraction) on Ca incorporation into secondary minerals as well as the complexities associated with replicating natural weathering processes in the laboratory.

To advance understanding of Ca isotopic fractionation during chemical weathering we measured $\delta^{44/40}$Ca values in a well-characterized weathering profile through saprolites formed on a metadiabase dike. These samples were previously analyzed for their mineralogy, bulk density, major and trace elements (Gardner et al., 1981), Li (Rudnick et al., 2004), Mg (Teng et al., 2010a), Cu (Liu et al., 2014) and Mo stable isotopes (Greaney et al., 2021). The $\delta^{44/40}$Ca variability in the saprolites is evaluated in terms of aeolian dust addition, selective weathering of rock-forming minerals, and formation of clay minerals.

2. Samples

The saprolites analyzed in this study developed on the Mesozoic subvertical Cayce metadiabase dike, which is exposed in a granite quarry near Cayce, South Carolina (Fig. 1). The 7 m thick unweathered metadiabase is dark grey to black in color and the dominant mineralogy is plagioclase (40%) and clinopyroxene (29%) with an unusually large amount of talc (20%) and chlorite (8%), reflecting incipient greenschist-facies metamorphism. The dike is cross-cut by 1-2 cm thick smectite veins. The saprolite formed during the Tertiary in a humid subtropical climate and is overlain by a thin coastal plain sediment of probable Tertiary age (Gardner et al., 1981) (Fig. 1). The upper 11 m of metadiabase dike is heavily weathered, below which fresh rock can been seen.

A mineralogical discontinuity occurs at 2 m depth in the saprolite profile (Gardner et al.,1981); above this discontinuity, siderite veins are not preserved but relict veins can be

seen. The saprolite here is characterized by kaolinite/smectite (K/S) ratios that decrease with more intense chemical weathering as density decreases. More specific clay species, such as montmorillonite, were not reported in Gardner et al. (1981). Enrichment of Fe^{3+} and formation of Fe-rich smectite (over kaolinite) in the upper 2 m suggests that oxidized conditions prevailed in the upper layer. By contrast, at depths below 2 m, kaolinite/smectite ratios increase with density and siderite veins are more commonly found. The latter formed by the weathering of original chlorite veins (Gardner et al., 1981). The appearance of siderite veins is interpreted to be the result of a redox change in the weathered profile from oxidizing conditions above 2 m, and more reducing conditions below this depth (Gardner et al., 1981). Reducing conditions below 2 m depth are also reflected by very low Fe content and formation of kaolinite over Al-rich smectite. In the unweathered metadiabase, the blocks between the joints are free of siderite. The presence of a second discontinuity at 6 m depth, which possibly reflects the depth of a paleo-water table has been suggested based on a discontinuity seen in Al- normalized Li concentrations and Li isotopic studies (Rudnick et al., 2004), although similar discontinuities were not observed for Mg isotopes (Teng et al., 2010a).

Thirteen saprolite samples as well as one sample of the unweathered metadiabase were analyzed in this study. The fresh metadiabase sample was collected from a depth of 30 m within the quarry, well below the weathered zone. The saprolites were collected from the center of the dike using a metal cylinder (inner diameter = 5 cm) that was hammered into the saprolite to obtain a core. These samples were then pulverized (Gardner et al., 1981). The sampling locations are shown in Figure 1.

3. Analytical methods

Homogeneous powdered samples of the unweathered metadiabase and saprolites were dissolved using well-established laboratory protocols (Banerjee et al., 2016) in a clean laboratory at the Centre for Earth Sciences (CEaS), Indian Institute of Science (IISc), Bangalore. Briefly, 10 mg of each sample was dissolved in Savillex screw top flat-bottomed Teflon beakers using a 1:1 mixture of HF and HNO_3. The capped beakers were kept on a hot plate for 24 hours in a laminar flow fume hood. After 24 hours the samples were dried and redissolved in 1:1 HNO_3 and HCl and held for another 24 hours before removing the cap and drying. The dried samples were subsequently dissolved in HNO_3 and diluted 4000 times for trace element concentration measurements, which were measured using a quadrupole

Inductively Coupled Mass Spectrometer (ICPMS, Thermo Scientific X-Series II) at CEaS, IISc. United States Geological Survey (USGS) silicate rock standards BCR-2 (Columbia River basalt) and BHVO-2 (Hawaiian basalt) were used as calibration standards and AGV-2 (Andesite Guano Valley) was analysed as an unknown interspersed with the samples. A 10 ppb internal standard solution comprising Be, Cs, In, and Bi was introduced online to correct for instrumental drift. Analytical uncertainties, based on measurements of the AGV-2 standard as an unknown and replicate measurement of one sample, are better than 5%. Major element concentrations, measured on the same aliquots of powdered samples, were taken from published studies (Gardner et al., 1981). Titanium (Ti)-normalized Ca ($[Ca]_{Ti}$) and Mg ($[Mg]_{Ti}$) concentrations for the saprolite samples are calculated as $[X]_{Ti} = (X/Ti)_{saprolite}/(X/Ti)_{parent\ rock}$, where X = Ca, Mg.

For Ca isotopic measurements, powdered samples were dissolved using the above-mentioned acid-dissolution technique and a 10 ml stock solution containing 100 µg/g Ca was prepared for each sample. Following established laboratory protocols (Mondal and Chakrabarti, 2018), an aliquot of this stock solution containing 10 µg Ca was mixed with an appropriate amount of ^{43}Ca-^{48}Ca double spike in Teflon beakers. The sample-spike mixtures were kept at 80 ^{0}C for about 12 hours for equilibration. Calcium was separated from the sample-double spike mixtures by ion-exchange chromatography (AG-50W X8, 200-400 mesh resin) using 2.5 M HCl. Each sample was processed twice through the columns for complete separation of K from Ca. The Ca yields are between 80-90% while the procedural blanks for Ca are estimated to be less than 1 ng.

Approximately 5 µg of purified Ca was loaded with Ta_2O_5 as an activator on pre-degassed Ta filaments. Calcium isotope ratios were measured using a thermal ionization mass spectrometer (TIMS, Thermo Triton Plus) at CEaS, IISc, using a double filament assembly where Ta was used as the evaporation filament and Re as the ionization filament. Stable Ca isotopic compositions ($\delta^{44/40}Ca$) are reported relative to the NIST SRM915a $CaCO_3$ standard as $\delta^{44/40}Ca = (\delta^{44/40}Ca_{sample}/\ \delta^{44/40}Ca_{SRM915a} - 1) \times 1000$. The long-term external reproducibility of $\delta^{44/40}Ca$, based on analyses of multiple standards and replicate measurements of two samples (Table 1), is better than 0.08‰ (Mondal and Chakrabarti, 2018), which is considered as the two-sigma precision of the reported $\delta^{44/40}Ca$ values of the samples.

4. Results

The $\delta^{44/40}$Ca values of the unweathered metadiabase and saprolites are reported in Table 1. During this study, multiple measurements of the standards NIST SRM 915a and NASS-6 seawater yielded $\delta^{44/40}$Ca values of 0.01 $\pm$ 0.05 (2SD, n = 3) and 1.88 $\pm$ 0.08 (2SD, n = 4), respectively (Table 1). The $\delta^{44/40}$Ca value of the unweathered metadiabase is 0.98‰, which overlaps the bulk silicate Earth value, while all but one of the saprolites have higher $\delta^{44/40}$Ca values, ranging from 0.99‰ to 1.26‰ (Table 1). Selected trace element concentrations of the unweathered metadiabase and the saprolite samples are reported, along with previously reported major element (oxide) concentrations (Gardner et al., 1981; Rudnick et al., 2004) in Table 1. The $\delta^{44/40}$Ca values of the saprolites decrease progressively with depth, although not monotonically, and the compositions of two saprolites collected from > 6 m depths overlap, within uncertainty, the $\delta^{44/40}$Ca value of the unweathered metadiabase (Fig. 2). The $\delta^{44/40}$Ca values correlate negatively with bulk density and Ti-normalized Ca concentrations ($[Ca]_{Ti}$) and positively with the chemical index of alteration (CIA) values (defined as molar $Al_2O_3/Al_2O_3+CaO+K_2O+Na_2O$) (Nesbitt and Young, 1982; McLennan, 1993) (Fig. 3). The Th/Nb ratios in the saprolites are systematically higher (0.46-0.61) than those of the unweathered metadiabase (0.39, Table 1, Fig. 4). In plots of $\delta^{44/40}$Ca versus Al/Ca and Sr/Ca, the saprolites do not plot on a trend defined by mixing of clinopyroxene and plagioclase end members (Fig. 5).

The $\delta^{44/40}$Ca values of the saprolites correlate positively with δ^{26}Mg (Teng et al., 2010a) and negatively with δ^{7}Li values (Rudnick et al., 2004) (Fig. 6). The CIA values of the saprolites increase with increasing ratio of kaolinite to Al-rich smectite in the saprolites (Gardner et al., 1981) while $[Ca]_{Ti}$ decreases with increasing kaolinite/smectite (Fig. 7a). However, four samples collected from shallower depths (< 2 m) fall off this trend (Fig. 7a, circled) with relatively low kaolinite/smectite at high CIA values. These four samples have high Fe_2O_3 (Table 1) and are enriched in Fe-smectite. The $\delta^{44/40}$Ca values of the saprolites are higher in samples with high kaolinite/smectite (Fig. 7b). However, the four samples collected from shallower depths (< 2 m) that are enriched in Fe-smectite with relatively low kaolinite/smectite, also display high $\delta^{44/40}$Ca values (Fig. 7b).

5. Discussion

The saprolites show significant and systematic variability in their $\delta^{44/40}$Ca values (0.91‰ to 1.26‰), which are higher than that of the unweathered metadiabase (0.98‰), save for one sample (Table 1). Several processes may have influenced the $\delta^{44/40}$Ca of the saprolites,

including radiogenic ^{40}Ca ingrowth, sample powder heterogeneity, vegetative input, addition of seawater aerosols, aeolian dust addition, selective mineralogical weathering, and development of secondary minerals. We address each of these, in turn.

5.1 Radiogenic ingrowth, mineralogical heterogeneity, vegetation, and sea-spray

Radiogenic ingrowth of ^{40}Ca resulting from the beta decay of ^{40}K, which has a half-life of 1.25 billion years (Steiger and Jager, 1977), can lower the $\delta^{44/40}Ca$ values of samples. However, radiogenic ingrowth is important only for samples with high K/Ca (>1) that are older than a billion years (Fantle and Tipper, 2014). The low K/Ca in the samples of this study (K/Ca < 1, Gardner et al., 1981) and their Mesozoic age (Teng et al., 2010) rules out the influence of radiogenic ^{40}Ca ingrowth in the samples of this study. Additionally, radiogenic ingrowth of ^{40}Ca lowers the measured $\delta^{44/40}Ca$ value of samples from their true value, which is the opposite of what is observed. Collectively, these observations suggest negligible influence of radiogenic ^{40}Ca on the $\delta^{44/40}Ca$ values.

The observed isotopic variability in the saprolites is unlikely to be due to mineralogical heterogeneity within the sample powders. Repeat dissolution and analysis of two saprolite samples (M11 and M12) yielded $\delta^{44/40}Ca$ values that are within the long-term analytical uncertainty of 0.08 ‰ (2SD), which suggests that the powdered saprolite samples are homogeneous. Moreover, if the variability in $\delta^{44/40}Ca$ values of the saprolites were due to sample powder heterogeneity, one would not expect to see the correlations between $\delta^{44/40}Ca$ and depth, bulk density, CIA, and other stable isotopes (e.g., Li and Mg, Fig. 7). Likewise, the unweathered metadiabase is a fine-grained metaigneous rock and, although only one sample of this rock was analysed, sample powder heterogeneity is unlikely to have influenced the $\delta^{44/40}Ca$ value of the metadiabase, which is similar to that of mantle-derived basalts and the BSE (Kang et al., 2017) (Fig. 2).

Calcium isotope variability in soils can be caused by the uptake of light isotopes by vegetation, and the supply of ^{40}Ca-enriched inputs to the soil from litterfall and atmospheric deposition (Cenki-Tok et al., 2009; Griffith et al., 2020). During bio-lifting, plants preferentially take up lighter isotopes of Ca and hence, produce a trend of increasing $\delta^{44/40}Ca$ with increasing depth (Bullen and Chadwick, 2016; Schmitt et al., 2017). This is the opposite of the trend in $\delta^{44/40}Ca$ observed in the saprolites of this study (Fig. 2). Additionally, there are no reports of remnants of plant material in the Cayce saprolites, consistent with sampling from depths of at least a meter below the coastal plain sediments (Fig. 1). These observations

suggest that vegetation has had little influence on the $\delta^{44/40}$Ca variability seen in these saprolites.

The Cayce saprolites are located ~200 km from the Atlantic coast and their composition could potentially be affected by sea spray. However, sodium concentrations in the samples are extremely low, mostly below detections limits (Gardner et al., 1981), which rules out the effect of sea spray on the Ca isotopic composition of these samples. We now turn to the possible influences of aeolian dust addition, selective weathering of rock-forming minerals, and secondary mineral formation.

5.2 Aeolian dust addition

We next investigate whether the $\delta^{44/40}$Ca variability in the saprolites can be explained by addition of aeolian dust. Thorium is highly incompatible and concentrated in the upper continental crust and therefore acts as a good proxy to fingerprint aeolian dust addition. The variation in Th concentrations in the saprolites, corrected for possible fluid-loss using the fluid immobile Nb, when compared relative to the unweathered metadiabase can be used to investigate the addition of aeolian dust and its effect on stable calcium isotope compositions of the saprolites. The fraction of added dust can be calculated from the following equations:

$$f_{dust}^{Th} = \frac{\frac{Nb}{Th}_{saprolite} - \frac{Nb}{Th}_{metadiabase}}{\frac{Nb}{Th}_{dust} - \frac{Nb}{Th}_{metadiabase}} \quad (1)$$

$$F_{dust} = \frac{f_{dust}^{Th} * [Th]_{saprolite}}{[Th]_{dust}} \quad (2)$$

Equation 1 quantifies the mass fraction (f_{dust}^{Th}) (based on molar ratios) of dust-derived Th in the saprolites while equation 2, which is a continuation from equation 1, calculates the mass fraction of dust (F_{dust}) (gm/ gm) in the saprolites (adapted from Babechuk et al., 2015). It may be noted that for calculation of f_{dust}^{Th}, the denominator should be Th.

The Th/Nb ratios in the saprolites range from 0.46-0.61 (Nb/Th = 1.64 - 2.17), which are higher than that of the unweathered metadiabase (0.39, Nb/Th = 2.56, Table 1, Fig. 4). For our calculations, the Th and Nb concentrations of the aeolian dust end member is assumed to be same as those of loess (Gallet et al., 1998; Barth et al., 2000; Chauvel et al., 2014). The average Th concentration of loess is 11.15 µg/g and average Nb concentration is 13 µg/g, making its Th/Nb = 0.86 (Barth et al., 2000). Using these compositions for the aeolian dust, our calculations indicate that the saprolite samples may contain between 3-11% aeolian dust

(F_{dust}), with saprolite M13 showing the highest proportion of dust (Fig. 4, Table 1). With only 3-11 wt% contribution of aeolian dust, the Ca concentration of the aeolian dust end member would have to be very high, along with an unusually high $\delta^{44/40}$Ca value, to explain the isotopic compositions of the saprolites. Simple mass balance calculations (Table S1) indicate that for the CaO concentrations observed in loess, ranging from 0.45-10.9 wt% (Gallet et al., 1998), the $\delta^{44/40}$Ca value of the aeolian dust would need to be 2.7 - 119 ‰ to explain the isotopically heavy saprolites near the top of the profile (Table S1), which is higher than any measured materials from Earth (Fantle and Tipper, 2014). While there are no reported $\delta^{44/40}$Ca data for aeolian dust or loess, such high $\delta^{44/40}$Ca values are extremely unlikely. For example, the $\delta^{44/40}$Ca values of surface sediments from dust-producing regions like the Black Rock Desert are ~0.78 ‰ (Fantle et al., 2012). Moreover, this dust is derived from the upper continental crust, which is enriched in K, and therefore radiogenic ingrowth of ^{40}Ca in such samples should lower the $\delta^{44/40}$Ca values (e.g., Fantle and Tipper et al., 2014); hence, aeolian dust addition likely had limited influence on the $\delta^{44/40}$Ca values of the saprolites, and, if anything, may have made them isotopically lighter than their dust-free counterparts.

5.3 Chemical weathering

Chemical weathering of the Cayce metadiabase dike led to the dissolution of primary minerals and formation of secondary minerals like Al-rich smectite, kaolinite, as well as Fe-rich smectite (Gardner et al., 1981). The abundances of these secondary minerals change with depth in the profile and reflect unique formation processes under changing redox conditions and chemical weathering intensity. Saprolites collected from >6 m depth display greater variability in compositions and record signatures of relatively less intense weathering, including lower CIA, higher $[Ca]_{Ti}$, as well as higher bulk density (Table 1). By contrast, saprolites collected from the upper 6 m have low $[Ca]_{Ti}$ as well as low bulk density, which are consistent with their high CIA values and suggest pervasive leaching and loss of soluble elements like calcium into the hydrosphere during weathering (Table 1).

Calcium isotope fractionation during chemical weathering is influenced by mineral dissolution and secondary mineral formation (e.g., Chapman et al., 2009; Ryu et al., 2011; Banerjee and Chakrabarti, 2018; Griffith et al., 2020). The $\delta^{44/40}$Ca values of the saprolites decrease with depth in the profile, approaching the $\delta^{44/40}$Ca value of the unweathered metadiabase (Fig. 3b). The negative correlation between $\delta^{44/40}$Ca values and bulk density and $[Ca]_{Ti}$, and the positive correlation with CIA values (Fig. 3) suggest that the variation in

$\delta^{44/40}$Ca values of saprolites results from chemical weathering; specifically, these trends suggest that $\delta^{44/40}$Ca values increase with increasing degree of chemical weathering. Earlier studies have suggested the presence of a palaeowater table at 6 m depths (Rudnick et al., 2004). This compositional discontinuity at 6 m depth is also observed in depth profiles of CIA, $[Ca]_{Ti}$, and bulk density (Table 1), but $\delta^{44/40}$Ca values show a continuous change with depth, with no discontinuity across this boundary (Table 1, Fig. 2). This continuous change in $\delta^{44/40}$Ca values of the saprolites with depth was also observed for the δ^{26}Mg values of these samples (Teng et al., 2010a).

We next investigate exactly how chemical weathering influenced the saprolites - whether through selective dissolution of rock-forming minerals, and/or due to the formation of secondary phases such as clays.

5.3.1 Selective dissolution of rock-forming minerals

The two most abundant minerals in the unweathered metadiabase are plagioclase feldspar (fs) and clinopyroxene (cpx). Clinopyroxene is more susceptible to dissolution than plagioclase. Since only powdered samples of the unweathered metadiabase were available, separation of plagioclase and clinopyroxene from the metadiabase could not be performed. Using previously analyzed igneous cpx and fs, we construct a simple mixing curve between $\delta^{44/40}$Ca and Al/Ca (Figure 5a) and $\delta^{44/40}$Ca and Sr/Ca (Figure 5b). The parameters and equations for the mixing calculations have been taken from Banerjee and Chakrabarti (2018) (Table S2). The theoretical stable calcium composition of a saprolite sample formed by selective mineral dissolution can be given as:

$$\delta^{44/40}Ca_{saprolite} = (f_{plag} * \delta^{44/40}Ca_{plag} * [Ca]_{plag} + (1- f_{plag}) * \delta^{44/40}Ca_{cpx} * [Ca]_{cpx}) / (f_{plag} * [Ca]_{plag} + (1- f_{plag}) * [Ca]_{cpx}) \quad (3)$$

Where, f and [Ca] are the weight fraction of the mineral (plagioclase or clinopyroxene) and its corresponding concentration (µg/g), respectively.

Similar equations can be constructed using $(Al/Ca)_{saprolite}$ and $(Sr/Ca)_{saprolite}$. The calculations are presented in Table S2. The mixing curves between $\delta^{44/40}$Ca and Sr/Ca (Fig. 5a) and Al/Ca (Fig. 5b) generated using the above equations do not intersect the compositions of the saprolites and are independent of the starting $\delta^{44/40}$Ca composition (within observed natural range) of plagioclase or clinopyroxene. This result indicates that the $\delta^{44/40}$Ca variability in the

saprolites cannot be explained by selective dissolution of the original igneous minerals in the metadiabase.

Further evidence against selective dissolution of clinopyroxene for explaining the range of $\delta^{44/40}Ca$ of the saprolites can be had from examining the behavior of Ca isotopes in igneous rocks. Large inter-mineral fractionation exists between igneous mineral pairs ($\Delta^{44}Ca = \delta^{44/40}Ca_a - \delta^{44/40}Ca_b$ ~2.5 ‰, where 'a' and 'b' are two different minerals, Antonelli and Simon, 2020). While the $\delta^{44/40}Ca$ values of feldspar and clinopyroxene show significant variability (e.g., Huang et al., 2010; Chen et al., 2018; Antonelli et al., 2019; Wang et al., 2019; Dai et al., 2020), their $\delta^{44/40}Ca$ values are typically lower than or equal to the BSE value of 0.94 ‰. Interestingly, the $\Delta^{44/40}Ca_{cpx\text{-}fs}$ values typically range from 0-0.3‰ (Antonelli et al., 2019). Selective dissolution of clinopyroxene will decrease the $\delta^{44/40}Ca$ values of the saprolites to below that of the BSE value, which is opposite to what is observed in the saprolites. Hence, selective dissolution of rock-forming minerals cannot explain the saprolite $\delta^{44/40}Ca$ values and other processes are necessary to explain the high $\delta^{44/40}Ca$ of the saprolites.

5.4 Clay minerals

Adsorption of water-soluble metal ions onto secondary minerals may produce significant fractionation of stable isotopes. Heavier isotopes of Mg are incorporated in natural clays (illite, montmorillionite and kaolinite) and brucite (Wimpenny et al., 2014; Ryu et al., 2016); however, laboratory experiments on brucite (Li et al., 2014) and smectite group of minerals (Hindshaw et al., 2020) show enrichment of lighter isotopes of Mg. Enrichment of heavier isotopes of Mg, as seen in natural clays, has been observed in soils (Pogge von Strandmann et al., 2012), where chemical weathering leads to leaching of lighter Mg isotopes into the hydrosphere, leaving behind a regolith enriched in heavier Mg isotopes (Teng et al., 2010a; Liu et al., 2014). Lighter isotopes of Mo are preferentially retained by accessory Fe-oxy-hydroxides and clay (Greaney et al., 2021) and lighter isotopes of Ba are incorporated into or adsorbed onto Fe-Mn oxydydroxides (Gong et al., 2019).

Calcium isotope data from experimental studies of clay minerals record variable results. Ockert et al. (2013) showed that the exchangeable (adsorbed) fraction of Ca in illite and kaolinite incorporates lighter Ca isotopes relative to the fluid, but these experiments were done in the presence of ammonium, which greatly enhances isotopic fractionation. While ammonium is common in the marine pore fluids that were the target of the Ockert et al.

(2013) study, ammonium is generally absent in terrestrial weathering environments. The ammonium-free experiments of Ockert et al. (2013) showed virtually no Ca isotope fractionation during adsorption onto clays. Similarly, Brazier et al. (2019) found no significant Ca isotope fractionation during desorption or adsorption on kaolinite, while montmorillonite preferentially adsorbed lighter isotopes of calcium. The nature of Ca isotope fractionation accompanying structural incorporation of Ca into clays has not yet been studied. Also, there are no available data for Ca isotopic fractionation during formation of clays in natural soils.

A positive correlation between $\delta^{44/40}$Ca and δ^{26}Mg values of the Cayce metadiabase saprolites (Fig. 6a) suggests that Ca and Mg isotopes behave similarly during chemical weathering. Given that heavier isotopes of Mg are incorporated into natural clays (Wimpenny et al., 2014; Ryu et al., 2016), a positive correlation between $\delta^{44/40}$Ca and δ^{26}Mg values could be interpreted as preferential uptake of the heavier isotopes of calcium by clay minerals relative to the hydrosphere. Although Ca is a relatively minor constituent of clay minerals, positive correlations between Ti-normalized Ca ($[Ca]_{Ti}$) and Mg ($[Mg]_{Ti}$) concentrations (Fig. S1a) indicates similar behavior of these elements during saprolitizaion. Furthermore, negative correlations between $\delta^{44/40}$Ca and $[Ca]_{Ti}$ (Fig. 3b) and $\delta^{44/40}$Ca and $[Mg]_{Ti}$ (Fig. S1b) indicates that with loss of Ca and Mg, the saprolites are progressively enriched in the heavier isotopes of Ca. The negative trend between $\delta^{44/40}$Ca and $[Ca]_{Ti}$ (Fig. 3b) further suggests that Ca loss during chemical weathering is far greater than Ca uptake during secondary mineral formation. Formation of saprolite is a complex process. The $\delta^{44/40}$Ca values of the saprolites represent the final signature of processes involving primary mineral dissolution and formation of secondary minerals. Nevertheless, Ca loss during saprolite formation can be visualised using a simple Rayleigh distillation model (Fig. S2); most of the saprolites lie on model curves with apparent fractionation factor, α, ranging from 1.00005-1.00015. A similar exercise for Mg isotopic fractionation in the same saprolite samples yielded α values ranging from 1.00005-1.0004 (Teng et al., 2010a).

In contrast to Mg and Ca isotopes, heavier isotopes of Li preferentially partition into water during weathering (Pistiner and Henderson, 2003), driving the δ^{7}Li of saprolites to low values (Rudnick et al., 2004; Tong et al., 2021). Additionally, Li isotope studies on natural and synthesized trioctahedral clays show that ^{6}Li is preferentially incorporated into the clays (Vigier et al., 2008; Hindshaw et al., 2019). A negative correlation between $\delta^{44/40}$Ca and δ^{7}Li

values (Rudnick et al., 2004) in the Cayce metadiabase saprolites (Fig. 6b) suggests that, while the combined process of weathering and secondary mineral formation drives the δ^{7}Li of saprolites to low values, the $\delta^{44/40}$Ca values increase, again suggesting that clay minerals preferentially incorporate the heavier isotopes of calcium, overwhelming the influence of dust addition. The linear trend between the different stable isotopic systems, as observed in the Cayce metadiabase saprolites has also been observed for Li and Mg isotopes in experimental studies on high-Mg stevensite clays (Hindshaw et al., 2011; Hindshaw et al., 2019). However, the relative incorporation of Ca, Mg, and Li and other metals in clays, the exact sites of incorporation (structural and/or exchange layers), and the corresponding isotopic fractionation factors remain to be investigated.

Three different clays are found in the Cayce metadiabase saprolite: Fe-rich smectite (restricted to the upper 2 m, samples M1, M3, M5, and M6, Table 1), Al- rich smectite, and kaolinite. The Fe-rich smectite formed as a result of late-stage processes when Fe^{3+} reacted with Al-rich smectite or kaolinite (Gardner et al., 1981). Saprolites with higher CIA values have high kaolinite/smectite (Fig. 7a), consistent with increased kaolinization and loss of soluble elements with increasing degree of chemical weathering. With increasing kaolinite/smectite, the Ca concentration decreases in saprolites, consistent with loss of fluid-mobile Ca with increased kaolinitization (Fig 7a). Samples with high kaolinite/smectite, barring the Fe-rich smectites, also display high $\delta^{44/40}$Ca (Fig. 7b). The above trends further suggest that loss of Ca with increasing weathering (high CIA) and kaolinitization (high kaolinite/smectite) results in loss of the lighter isotopes of Ca from the smectite structure to the hydrosphere thereby leaving the residual clays enriched in the heavy isotopes of Ca. Interestingly, Mg concentrations in the saprolites also decrease with increasing kaolinite/smectite while the δ^{26}Mg values increase with increasing kaolinite/smectite (excluding the Fe-rich smectites, Fig S3). Overall, the similar trends between Ca and Mg concentrations as well as $\delta^{44/40}$Ca and δ^{26}Mg with kaolinite/smectite indicate that high $\delta^{44/40}$Ca in the saprolites are best explained by enrichment of heavy isotopes of Ca in clay minerals.

The discrepancy between observations from natural clay-rich samples (this study) and experimental studies on Ca adsorption on clays (Okert et al., 2013; Brazier et al., 2019) suggests that Ca isotope fractionation is strongly dependent on the bonding environment of Ca, and that Ca discriminates between ionic bonding within mineral sites versus electrostatic

bonding associated with adsorption. This highlights the need for site-specific Ca isotope fractionation studies like that of Hindshaw et al. (2019) for Li.

Four samples from the upper 2 m that contain Fe-rich smectite fall off the trends described above (circled in Figs. 7 and S3); these samples display relatively low kaolinite/smectite and low Al_2O_3 but high CIA, Fe_2O_3, as well as $\delta^{44/40}$Ca and δ^{26}Mg values. This suggests that such Fe-rich smectites may produce considerable Ca and Mg isotopic fractionation. Overall, our results indicate that the formation of clay minerals in the saprolite developed on the Cayce metadiabase best explains the $\delta^{44/40}$Ca variability observed in these samples.

6. Conclusions

The $\delta^{44/40}$Ca values of saprolites developed on the Mesozoic Cayce metadiabase dike in South Carolina are higher than that of the unweathered metadiabase and systematically increase with decreasing depths and with increasing CIA values, decreasing bulk density and $[Ca]_{Ti}$. These data document progressive loss of light isotopes of Ca to the hydrosphere during chemical weathering. Addition of aeolian dust is limited to <11 wt.% based on mass balance of incompatible, insoluble trace elements (i.e., Th/Nb ratio). Our calculations show that dust addition and/or selective weathering of rock-forming minerals, which typically have $\delta^{44/40}$Ca values that overlap with or are slightly lower than the BSE value of 0.94 ‰, cannot explain the high $\delta^{44/40}$Ca values (> 1 ‰) observed in the saprolites. The $\delta^{44/40}$Ca values of the saprolites correlate positively with δ^{26}Mg and negatively with δ^{7}Li values published for the same samples, suggesting that secondary mineral formation is the main driver of Ca stable isotope fractionation. Calcium isotope fractionation in saprolites and associated progressive loss of Ca can be modeled using Rayleigh distillation, with apparent fractionation factors between saprolites and fluid (α) of 1.00005 to 1.00015. Barring a few Fe-rich smectites from < 2 m depth, the $\delta^{44/40}$Ca values of the saprolites increase with increasing kaolinite/smectite ratio while the $[Ca]_{Ti}$ decreases with increasing kaolinite/smectite and these trends are similar for δ^{26}Mg and Mg concentrations versus kaolinite/smectite ratio of these samples.

The high $\delta^{44/40}$Ca values in the saprolites reflect loss of lighter Ca isotopes to the hydrosphere during kaolinitization. The Fe-rich smectites show enrichments in heavy Ca, with $\delta^{44/40}$Ca values overlapping those observed in kaolinite-rich samples. The enrichment of the heavier isotopes of Ca in Fe-rich smectites relative to Al-rich smectites may reflect the influence of Fe in the structure of clays on Ca isotopic fractionation. Our results contrast with laboratory

adsorption experiments, which broadly show either no isotopic fractionation associated with clays, or that lighter isotopes of Ca are preferentially adsorbed by clays. This discrepancy may suggest that Ca isotope fractionation varies between ionic bonding within mineral sites versus electrostatic bonding in the case of adsorption and highlights the need for site-specific isotope fractionation studies. It also suggests that it is Ca in the clay structure that dominates the isotope fractionation produced during continental weathering.

Acknowledgements

We are grateful for the comments and suggestions of Matthew Fantle and an anonymous reviewer on earlier versions of this manuscript, which helped us to improve the presentation. RC acknowledges partial funding from DST-SERB (CRG/2018/004254). UH acknowledges salary support from UGC. We dedicate this work to the memory of Bob Gardner, who collected and initially characterized these samples.

Figure captions

Fig. 1. Schematic diagram showing the cross-section of the Mesozoic Cayce metadiabase dike intruded in granite (after Gardner et al., 1981). A layer (~4 m) of sandy, Tertiary coastal sediments overlies the dike. The unweathered metadiabase sample (UW) is denoted with a filled green star while the saprolite samples are denoted with filled red circles.

Fig 2. Variation in $\delta^{44/40}$Ca values of the saprolites plotted versus sampling depth. The saprolite samples above 6 m are more weathered and show a higher $\delta^{44/40}$Ca values. The unweathered metadiabase (green star) is sampled at a depth of 30 m and its $\delta^{44/40}$Ca value overlaps that of the Bulk Silicate Earth (BSE, Kang et al., 2017). The error bar reflects the external reproducibility of $\delta^{44/40}$Ca (2SD) while the vertical grey bar denotes the composition of the BSE.

Fig. 3. $\delta^{44/40}$Ca values of saprolites (red filled circles) and the unweathered metadiabase (green filled star) relative to (a) Chemical Index of alteration (CIA), (b) Ti normalized Ca concentrations ($[Ca]_{Ti}$), and (c) bulk density of the samples. The $\delta^{44/40}$Ca values increase with increasing CIA and decreasing $[Ca]_{Ti}$ and bulk density, which is consistent with the loss of mobile elements like calcium, and preferential loss of the lighter isotopes of calcium during weathering. The error bars reflect the external reproducibility of $\delta^{44/40}$Ca (2SD) while the grey bars denote the composition of the BSE.

Fig. 4. Th/Nb ratio of the unweathered metadiabase (UW, green filled star) shows lower values than the saprolites (filled circles) suggesting contribution from aeolian dust, whose composition has been approximated by the Th/Nb composition of average loess (0.86, Barth et al., 2000). However, mass balance calculations indicate minimal influence from aeolian dust, with calculated weight percent ranging between 3% to 11% (filled squares). See text for details.

Fig. 5. Plots of $\delta^{44/40}$Ca values versus (a) Sr/Ca and (b) Al/Ca of the saprolites and unweathered metadiabase (UW). The saprolites plot beyond the mixing trends (blue line) between compositions of clinopyroxene and plagioclase indicating that selective mineral dissolution cannot explain the observed variability in $\delta^{44/40}$Ca of the saprolites. Data for mineral end members are taken from Banerjee and Chakrabarti (2018). See text for details.

Fig. 6. Correlations between $\delta^{44/40}$Ca and (a) δ^{26}Mg and (b) δ^{7}Li values of the saprolites and the unweathered metadiabase sample. A rough positive correlation between $\delta^{44/40}$Ca and δ^{26}Mg values suggests that lighter isotopes of both Ca and Mg are leached into the hydrosphere during weathering leaving the residue enriched in the heavier isotopes. A negative trend between $\delta^{44/40}$Ca and δ^{7}Li suggests that, in contrast to Ca and Mg isotopes, the heavier isotope of Li is leached into the hydrosphere leaving the residue enriched in the lighter isotope. The δ^{26}Mg and δ^{7}Li values of the samples are taken from Teng et al. (2010) and Rudnick et al. (2004), respectively. The error bars reflect the external reproducibility (2SD) of $\delta^{44/40}$Ca, δ^{26}Mg and δ^{7}Li while the grey boxes denote the estimated compositions of the BSE (Ca: Kang et al., 2017, Li: Penniston-Dorland et al., 2017 and references therein; Mg: Teng et al., 2010b).

Fig. 7. (a). The CIA values of the saprolite samples (filled circles) plotted against kaolinite to Al-rich smectite ratio (K/S, data taken from Gardner et al., 1981). Also plotted are the Ti normalised Ca concentrations ($[Ca]_{Ti}$) of the saprolites (circles with cross hairs) versus K/S. Samples with low $[Ca]_{Ti}$ display high CIA values, consistent with Ca loss during weathering. The unweathered metadiabase (UW) has K/S = 0, which suggests no clay formation. Saprolites with higher CIA values typically display higher kaolinite/smectite. However, four saprolite samples collected from shallower depths (< 2 m, circled) fall off this trend, displaying relatively low kaolinite/smectite at high CIA values. These samples are enriched in Fe-smectite (within red oval). (b) The $\delta^{44/40}$Ca values of the saprolites are higher in samples with high kaolinite/smectite. However, the four samples collected from shallower

depths (< 2 m, circled) that are enriched in Fe-smectite have relatively low kaolinite/smectite, and high $\delta^{44/40}$Ca values. See text for discussion. The error bar reflects the external reproducibility of $\delta^{44/40}$Ca (2SD) while the grey bar denotes the composition of the BSE.

References

Amini, M., Eisenhauer, A., Böhm, F., Fietzke, J., Bach, W., Garbe-Schönberg, D., Rosner, M., Bock, B., Lackschewitz, K.S. and Hauff, F., 2008. Calcium isotope ($\delta^{44/40}$Ca) fractionation along hydrothermal pathways, Logatchev field (Mid-Atlantic Ridge, 14° 45′ N). *Geochimica et Cosmochimica Acta*, *72*(16), pp.4107-4122.

Antonelli, M.A., Schiller, M., Schauble, E.A., Mittal, T., DePaolo, D.J., Chacko, T., Grew, E.S. and Tripoli, B., 2019. Kinetic and equilibrium Ca isotope effects in high-T rocks and minerals. *Earth and Planetary Science Letters*, *517*, pp.71-82.

Antonelli, M.A. and Simon, J.I., 2020. Calcium isotopes in high-temperature terrestrial processes. *Chemical Geology*, *548*, p.119651.

Babechuk, M. G., Widdowson, M., Murphy, M., and Kamber, B. S., 2015. A combined Y/Ho, high field strength element (HFSE) and Nd isotope perspective on basalt weathering, Deccan Traps, India. *Chemical Geology*, 396, pp. 25-41.

Banerjee, A., Chakrabarti, R. and Mandal, S., 2016. Geochemical anatomy of a spheroidally weathered diabase. *Chemical Geology*, *440*, pp.124-138.

Banerjee, A. and Chakrabarti, R., 2018. Large Ca stable isotopic ($\delta^{44/40}$Ca) variation in a hand-specimen sized spheroidally weathered diabase due to selective weathering of clinopyroxene and plagioclase. *Chemical Geology*, *483*, pp.295-303.

Banerjee, A., Chakrabarti, R. and Simonetti, A., 2021. Temporal evolution of $\delta^{44/40}$Ca and $^{87}Sr/^{86}Sr$ of carbonatites: Implications for crustal recycling through time. *Geochimica et Cosmochimica Acta*, *307*, pp.168-191.

Barth, M.G., McDonough, W.F. and Rudnick, R.L., 2000. Tracking the budget of Nb and Ta in the continental crust. *Chemical Geology*, *165*(3-4), pp.197-213.

Blättler, C.L., Miller, N.R. and Higgins, J.A., 2015. Mg and Ca isotope signatures of authigenic dolomite in siliceous deep-sea sediments. *Earth and Planetary Science Letters*, *419*, pp.32-42.

Brazier, J.M., Schmitt, A.D., Gangloff, S., Pelt, E., Chabaux, F. and Tertre, E., 2019. Calcium isotopic fractionation during adsorption onto and desorption from soil phyllosilicates (kaolinite, montmorillonite and muscovite). *Geochimica et Cosmochimica Acta*, *250*, pp.324-347.

Bullen, T. and Chadwick, O., 2016. Ca, Sr and Ba stable isotopes reveal the fate of soil nutrients along a tropical climosequence in Hawaii. *Chemical Geology*, *422*, pp.25-45.

Cenki-Tok, B., Chabaux, F., Lemarchand, D., Schmitt, A.D., Pierret, M.C., Viville, D., Bagard, M.L. and Stille, P., 2009. The impact of water–rock interaction and vegetation on calcium isotope fractionation in soil-and stream waters of a small, forested catchment (the Strengbach case). *Geochimica et Cosmochimica Acta*, *73*(8), pp.2215-2228.

Chakrabarti, R., Mondal, S., Jacobson, A.D., Mills, M., Romaniello, S.J. and Vollstaedt, H., 2021. Review of techniques, challenges, and new developments for calcium isotope ratio measurements. *Chemical Geology*, p.120398.

Chapman, J.B., Weiss, D.J., Shan, Y. and Lemburger, M., 2009. Iron isotope fractionation during leaching of granite and basalt by hydrochloric and oxalic acids. *Geochimica et Cosmochimica Acta*, *73*(5), pp.1312-1324.

Chauvel, C., Garçon, M., Bureau, S., Besnault, A., Jahn, B.M. and Ding, Z., 2014. Constraints from loess on the Hf–Nd isotopic composition of the upper continental crust. *Earth and Planetary Science Letters*, *388*, pp.48-58.

Chen, C., Liu, Y., Feng, L., Foley, S.F., Zhou, L., Ducea, M.N. and Hu, Z., 2018. Calcium isotope evidence for subduction-enriched lithospheric mantle under the northern North China Craton. *Geochimica et Cosmochimica Acta*, *238*, pp.55-67.

Chen, B.B., Li, S.L., von Strandmann, P.A.P., Wilson, D.J., Zhong, J., Ma, T.T., Sun, J. and Liu, C.Q., 2023. Behaviour of Sr, Ca, and Mg isotopes under variable hydrological conditions in high-relief large river systems. *Geochimica et Cosmochimica Acta*.

Dai, W., Wang, Z., Liu, Y., Chen, C., Zong, K., Zhou, L., Zhang, G., Li, M., Moynier, F. and Hu, Z., 2020. Calcium isotope compositions of mantle pyroxenites. *Geochimica et Cosmochimica Acta*, *270*, pp.144-159.

Fantle, M.S., Tollerud, H., Eisenhauer, A. and Holmden, C., 2012. The Ca isotopic composition of dust-producing regions: Measurements of surface sediments in the Black Rock Desert, Nevada. *Geochimica et Cosmochimica Acta*, *87*, pp.178-193.

Fantle, M.S. and Tipper, E.T., 2014. Calcium isotopes in the global biogeochemical Ca cycle: Implications for development of a Ca isotope proxy. *Earth-Science Reviews*, *129*, pp.148-177.

Farkaš, J., Böhm, F., Wallmann, K., Blenkinsop, J., Eisenhauer, A., Van Geldern, R., Munnecke, A., Voigt, S. and Veizer, J., 2007. Calcium isotope record of Phanerozoic oceans: Implications for chemical evolution of seawater and its causative mechanisms. *Geochimica et Cosmochimica Acta*, *71*(21), pp.5117-5134.

Gardner, L.R., Kheoruenromne, I. and Chen, H.S., 1981. Geochemistry and mineralogy of an unusual diabase saprolite near Columbia, South Carolina. *Clays and Clay Minerals*, *29*(3), pp.184-190.

Gaschnig, R. M., Rudnick, E. L., McDonough, W. F., Kaufman, A. J., Valley, J. W., Hu, Z., Gao, S., Beck, M. L., 2016. Compositional evolution of the upper continental crust through time, as constrained by ancient glacial diamictites. *Geochimica et Cosmochimica Acta*, *186*, pp. 316-343.

Gallet, S., Jahn, B.M., Lanoë, B.V.V., Dia, A. and Rossello, E., 1998. Loess geochemistry and its implications for particle origin and composition of the upper continental crust. *Earth and Planetary Science Letters*, *156*(3-4), pp.157-172.

Gong, Y., Zeng, Z., Zhou, C., Nan, X., Yu, H., Lu, Y., Li, W., Gou, W., Cheng, W., Huang, F., 2019. Barium isotopic fractionation in latosol developed from strongly weathered basalt. *Science of the Total Environment*, 687, pp. 1295-1304.

Greaney, A.T., Rudnick, R.L., Romaniello, S.J., Johnson, A.C., Anbar, A.D. and Cummings, M.L., 2021. Assessing molybdenum isotope fractionation during continental weathering as recorded by weathering profiles in saprolites and bauxites. *Chemical Geology*, *566*, p.120103.

Griffith, E.M., Schmitt, A.D., Andrews, M.G. and Fantle, M.S., 2020. Elucidating modern geochemical cycles at local, regional, and global scales using calcium isotopes. *Chemical Geology*, *534*, p.119445.

Hindshaw, R.S., Reynolds, B.C., Wiederhold, J.G., Kretzschmar, R. and Bourdon, B., 2011. Calcium isotopes in a proglacial weathering environment: Damma glacier, Switzerland. *Geochimica et Cosmochimica Acta*, *75*(1), pp.106-118.

Hindshaw, R.S., Tosca, R., Goût, T.L., Farnan, I., Tosca, N.J. and Tipper, E.T., 2019. Experimental constraints on Li isotope fractionation during clay formation. *Geochimica et Cosmochimica Acta*, *250*, pp.219-237.

Hindshaw, R.S., Tosca, R., Tosca, N.J. and Tipper, E.T., 2020. Experimental constraints on Mg isotope fractionation during clay formation: Implications for the global biogeochemical cycle of Mg. *Earth and Planetary Science Letters*, *531*, p.115980.

Huang, S., Farkaš, J. and Jacobsen, S.B., 2010. Calcium isotopic fractionation between clinopyroxene and orthopyroxene from mantle peridotites. *Earth and Planetary Science Letters*, *292*(3-4), pp.337-344.

Jacobson, A.D., Andrews, M.G., Lehn, G.O. and Holmden, C., 2015. Silicate versus carbonate weathering in Iceland: New insights from Ca isotopes. *Earth and Planetary Science Letters*, *416*, pp.132-142.

Kang, J.T., Ionov, D.A., Liu, F., Zhang, C.L., Golovin, A.V., Qin, L.P., Zhang, Z.F. and Huang, F., 2017. Calcium isotopic fractionation in mantle peridotites by melting and metasomatism and Ca isotope composition of the Bulk Silicate Earth. *Earth and Planetary Science Letters*, *474*, pp.128-137.

Kısakürek, B., Widdowson, M. and James, R.H., 2004. Behaviour of Li isotopes during continental weathering: the Bidar laterite profile, India. *Chemical Geology*, *212*(1-2), pp.27-44.

Lee, C.T.A., Morton, D.M., Little, M.G., Kistler, R., Horodyskyj, U.N., Leeman, W.P. and Agranier, A., 2008. Regulating continent growth and composition by chemical weathering. *Proceedings of the National Academy of Sciences*, *105*(13), pp.4981-4986.

Li, W., Beard, B.L., Li, C. and Johnson, C.M., 2014. Magnesium isotope fractionation between brucite [Mg $(OH)_2$] and Mg aqueous species: Implications for silicate weathering and biogeochemical processes. *Earth and Planetary Science Letters*, *394*, pp.82-93.

Liu, X.M. and Rudnick, R.L., 2011. Constraints on continental crustal mass loss via chemical weathering using lithium and its isotopes. *Proceedings of the National Academy of Sciences*, *108*(52), pp.20873-20880.

Liu, X.M., Teng, F.Z., Rudnick, R.L., McDonough, W.F. and Cummings, M.L., 2014. Massive magnesium depletion and isotope fractionation in weathered basalts. *Geochimica et Cosmochimica Acta*, *135*, pp.336-349.

Liu, S.A., Teng, F.Z., Li, S., Wei, G.J., Ma, J.L. and Li, D., 2014. Copper and iron isotope fractionation during weathering and pedogenesis: Insights from saprolite profiles. *Geochimica et Cosmochimica Acta*, *146*, pp.59-75.

Mondal, S. and Chakrabarti, R., 2018. A novel sample loading method and protocol for monitoring sample fractionation for high precision Ca stable isotope ratio measurements using double-spike TIMS. *Journal of Analytical Atomic Spectrometry*, *33*(1), pp.141-150.

McLennan, S.M., 1993. Weathering and global denudation. *The Journal of Geology*, *101*(2), pp.295-303.

Nan, X.Y., Yu, H.M., Rudnick, R.L., Gaschnig, R.M., Xu, J., Li, W.Y., Zhang, Q., Jin, Z.D., Li, X.H. and Huang, F., 2018. Barium isotopic composition of the upper continental crust. *Geochimica et Cosmochimica Acta*, *233*, pp.33-49.

Nelson, C.J., Jacobson, A.D., Kitch, G. D., and Weisenberger, T.B., 2021. Large calcium isotope fractionations by zeolite minerals from Iceland. *Communications Earth & Environment, 2, Article number 206*.

Nesbitt, H. and Young, G.M., 1982. Early Proterozoic climates and plate motions inferred from major element chemistry of lutites. *Nature*, *299*(5885), pp.715-717.

Ockert, C., Gussone, N., Kaufhold, S. and Teichert, B.M.A., 2013. Isotope fractionation during Ca exchange on clay minerals in a marine environment. *Geochimica et Cosmochimica Acta*, *112*, pp.374-388.

Penniston-Dorland, S., Liu, X-M. and Rudnick, R. L., 2017. Lithium isotope geochemistry. *Reviews in Mineralogy and Geochemistry*, *82(1)*, pp.165-217.

Pistiner, J.S. and Henderson, G.M., 2003. Lithium-isotope fractionation during continental weathering processes. *Earth and Planetary Science Letters*, *214*(1-2), pp.327-339.

Pogge von Strandmann, P.A.E., Opfergelt, S., Lai, Y.J., Sigfússon, B., Gislason, S.R. and Burton, K.W., 2012. Lithium, magnesium and silicon isotope behaviour accompanying weathering in a basaltic soil and pore water profile in Iceland. *Earth and Planetary Science Letters*, *339*, pp.11-23.

Rudnick, R.L. and Gao, S., 2003. 3.01-Composition of the continental crust. Treatise Geochem. 1, 1–64.

Rudnick, R.L., Tomascak, P.B., Njo, H.B. and Gardner, L.R., 2004. Extreme lithium isotopic fractionation during continental weathering revealed in saprolites from South Carolina. *Chemical Geology*, *212*(1-2), pp.45-57.

Ryu, J.S., Jacobson, A.D., Holmden, C., Lundstrom, C. and Zhang, Z., 2011. The major ion, $\delta^{44/40}$Ca, $\delta^{44/42}$Ca, and $\delta^{26/24}$Mg geochemistry of granite weathering at pH= 1 and T= 25° C: power-law processes and the relative reactivity of minerals. *Geochimica et Cosmochimica Acta*, *75*(20), pp.6004-6026.

Ryu, J.S., Vigier, N., Decarreau, A., Lee, S.W., Lee, K.S., Song, H. and Petit, S., 2016. Experimental investigation of Mg isotope fractionation during mineral dissolution and clay formation. *Chemical Geology*, *445*, pp.135-145.

Schmitt, A.D., Gangloff, S., Labolle, F., Chabaux, F. and Stille, P., 2017. Calcium biogeochemical cycle at the beech tree-soil solution interface from the Strengbach CZO (NE France): insights from stable Ca and radiogenic Sr isotopes. *Geochimica et Cosmochimica Acta*, *213*, pp.91-109.

Steiger, R.H., Jager, E., 1977. Subcommission on geochronology: convention on the use of decay constants in geo- and cosmochronology. *Earth and Planetary Science Letters*, 36, 359–362.

Tipper, E.T., Galy, A. and Bickle, M.J., 2006. Riverine evidence for a fractionated reservoir of Ca and Mg on the continents: implications for the oceanic Ca cycle. *Earth and Planetary Science Letters*, *247*(3-4), pp.267-279.

Teng, F.Z., Li, W.Y., Rudnick, R.L. and Gardner, L.R., 2010a. Contrasting lithium and magnesium isotope fractionation during continental weathering. *Earth and Planetary Science Letters*, *300*(1-2), pp.63-71.

Teng, F.Z., Ki, W-Y., Ke, S., Marty, B., Dauphas, N., Huang, S., Wu, F-Y. and Pourmand, A. 2010b. Magnesium isotopic composition of the Earth and chondrites. *Geochimica et Cosmochimica Acta*, *74*, pp. 4150-4166.

Teng, F.Z., McDonough, W.F., Rudnick, R.L., Dalpé, C., Tomascak, P.B., Chappell, B.W. and Gao, S., 2004. Lithium isotopic composition and concentration of the upper continental crust. *Geochimica et Cosmochimica Acta*, *68*(20), pp.4167-4178.

Teng, F.Z., Hu, Y., Ma, J.L., Wei, G.J. and Rudnick, R.L., 2020. Potassium isotope fractionation during continental weathering and implications for global K isotopic balance. *Geochimica et Cosmochimica Acta*, *278*, pp.261-271.

Tong, F., Xiao, Y., Sun, H., Wang, Y., Wan, H., Gou, L.F., Gong, Y., Huang, F., Li, D.Y. and Hou, Z., 2021. Lithium isotopic features of Quaternary basaltic saprolite, Zhanjiang, China: Atmospheric input and clay-mineral adsorption. *Science of The Total Environment*, *785*, p.147235.

Urey, 1952. Regarding the early history of the earth's atmosphere. *Geological Society of America Bulletin, 67, 1129-1128.*

Vigier, N., Decarreau, A., Millot, R., Carignan, J., Petit, S. and France-Lanord, C., 2008. Quantifying Li isotope fractionation during smectite formation and implications for the Li cycle. *Geochimica et Cosmochimica Acta*, *72*(3), pp.780-792.

Wang, Y., He, Y., Wu, H., Zhu, C., Huang, S. and Huang, J., 2019. Calcium isotope fractionation during crustal melting and magma differentiation: granitoid and mineral-pair perspectives. *Geochimica et Cosmochimica Acta*, *259*, pp.37-52.

Wimpenny, J., Colla, C.A., Yin, Q.Z., Rustad, J.R. and Casey, W.H., 2014. Investigating the behaviour of Mg isotopes during the formation of clay minerals. *Geochimica et Cosmochimica Acta*, *128*, pp.178-194.

Table 1. Data for unweathered Cayce metadiabase and overlying saprolites. Also reported are Ca isotopic compositions of standards (NASS6 seawater and NIST SRM 915a) analyzed during this study.

Sample	Depth	Density	kaolinite/smectite	CIA	SiO_2	Al_2O_3	Fe_2O_3	FeO*	MgO	CaO	K_2O	Na_2O	TiO_2	**Sr**	**Nb**	**Th**	**Th/Nb**	**Fraction of dust**	δ^{7}Li	δ^{26}Mg	**$\delta^{44/40}$Ca**
	m	g/cm3			wt%	wt%	wt%	wt%	wt%	wt%	wt%	wt%	wt%	**µg/g**	**µg/g**	**µg/g**					
											Saprolites										
M1	0.1	1	0.04	88	54.63	15.8	20.2		1.8	1	0.36	0	0.66	**36.26**	**2.12**	**1.02**	**0.48**	**0.03**	-11.6	0.53	**1.26**
M3	0.5	0.8	0.03	88	58.57	19.3	10.9	0.06	2.2	1	0.71	0	0.88	**43.67**	**2.85**	**1.73**	**0.61**	**0.11**	-10.1	0.62	**1.14**
M5	1.5	1	0.03	90	58.86	17.9	12.2	0.08	2	1.1	0.33	0	0.64	**40.84**	**1.61**	**0.85**	**0.53**	**0.04**	-14.4	0.59	**1.25**
M6	2	1	0.07	87	59.3	17.5	11.5	0.8	2	1	1.16	0	0.58	**51.27**	**2.19**	**1.09**	**0.50**	**0.04**	-12.1	0.61	**1.25**
M7	3	1	5	95	53.95	27.8	5.5	0.4	0.6	0.8	0.34	0	0.77	**25.02**	**2.52**	**1.23**	**0.49**	**0.04**	-13.8	0.3	**1.16**
M9	5	1.2	2.5	93	55.82	23.8	8.9	0.1	1	0.8	0.46	0	0.81	**34.79**	**2.59**	**1.27**	**0.49**	**0.05**	-17.3	0.4	**1.14**
M10	6	1.4	1.7	91	54.3	23.2	7.9	2.46	1	1.2	0.48	0	0.76	**34.75**	**2.69**	**1.57**	**0.58**	**0.09**	-20.2	0.07	**1.26**
M10 (replicate)														**37.32**	**2.82**	**1.64**	**0.58**				
M11	7	2.1	0.3	54	48.31	17.2	7.2	4.15	11.9	7.1	0.37	1.09	0.55	**44.40**	**2.33**	**1.39**	**0.59**	**0.08**	-6.7	-0.17	**1.04**
M11 (replicate)																					**1.02**
M12	8	2.3	0.15	55	49.38	18.2	8.8	3.8	8.6	7.2	0.43	1.33	0.56	**73.41**	**2.81**	**1.54**	**0.55**	**0.08**	-10.4	-0.11	**1.04**
M12																					**1.10**

(replicate)																				
M13	9	1.8	0.4	71	52.72	22.2	9.1	2.21	5.5	4	0.42	0.97	0.72	**53.08**	**3.03**	**1.81**	**0.60**	**0.11**	-11.8	0.02	**0.99**
L14-8	10	2.5	0.25	49	48.56	17.3	7.8	3.39	11	8.9	0.37	1.28	0.57	**51.55**	**2.64**	**1.21**	**0.46**	**0.03**	-9.1	-0.13	**1.03**
L14-9	10	2.5	0	46	49.11	16.9	7.1	3.98	10.5	9.5	0.39	1.36	0.58	**62.57**	**2.92**	**1.55**	**0.53**	**0.07**	-8.1	-0.31	**0.91**
M15	11	1.9	1	88	51.78	21.9	10.8	2.18	5.8	1.4	0.56	1.42	0.73	**45.76**	**2.49**	**1.30**	**0.52**	**0.06**	-13.7	-0.19	**n.a.**
M15 (replicate)														**45.5**	**2.49**	**1.32**	**0.53**				
											Metadiabase										
M20	30	3	0	45	48.68	17.1	7.1	6.26	11.8	10.4	0.32	0.43	0.78	**59.14**	**3.09**	**1.19**	**0.39**	**0**	-4.4	-0.22	**0.98**
AGV2 (nominal value)														**661 (659.5)**	**14.5 (14.12)**	**6.4 (6.17)**					
NASS6																					**1.88 ± 0.08 (n = 4)**
SRM915a																					**0.01 ± 0.05 (n = 3)**

Depth, bulk density, kaolinite/smectite ratio and major element concentrations are from Gardner et al. (1981).
CIA values, Li concentration and Li isotope data are from Rudnick et al. (2004).
Mg isotope data is from Teng et al. (2010).
Measurements performed as part of the present study are in bold
USGS standard AGV2 was run as unknown to check the quality of data. The nominal values, reported by GeoReM (http://georem.mpch-mainz.gwdg.de/ref_mat_pref_val.asp?refmatid=USGS+AGV-2), are shown in bracket against the measured concentration.
The two-sigma external precision of the reported $\delta^{44/40}Ca$ values of the samples is better than 0.08‰ based on analyses of standards.
n.a. = not analysed

The Authors declare that there is no conflict of interest.

Utpalendu Haldar

Ramananda Chakrabarti

Roberta L. Rudnick

Highlights

- Stable calcium isotopic compositions of Mesozoic Cayce Diabase saprolites from South Carolina
- Saprolites mostly show higher $\delta^{44/40}$Ca values compared to the unweathered diabase
- Loss of lighter isotopes of Ca during silicate weathering
- Dust addition and/or selective weathering of rock-forming minerals cannot explain the $\delta^{44/40}$Ca values of the saprolites
- Secondary clay mineral formation is the main driver of Ca stable isotope fractionation during silicate weathering

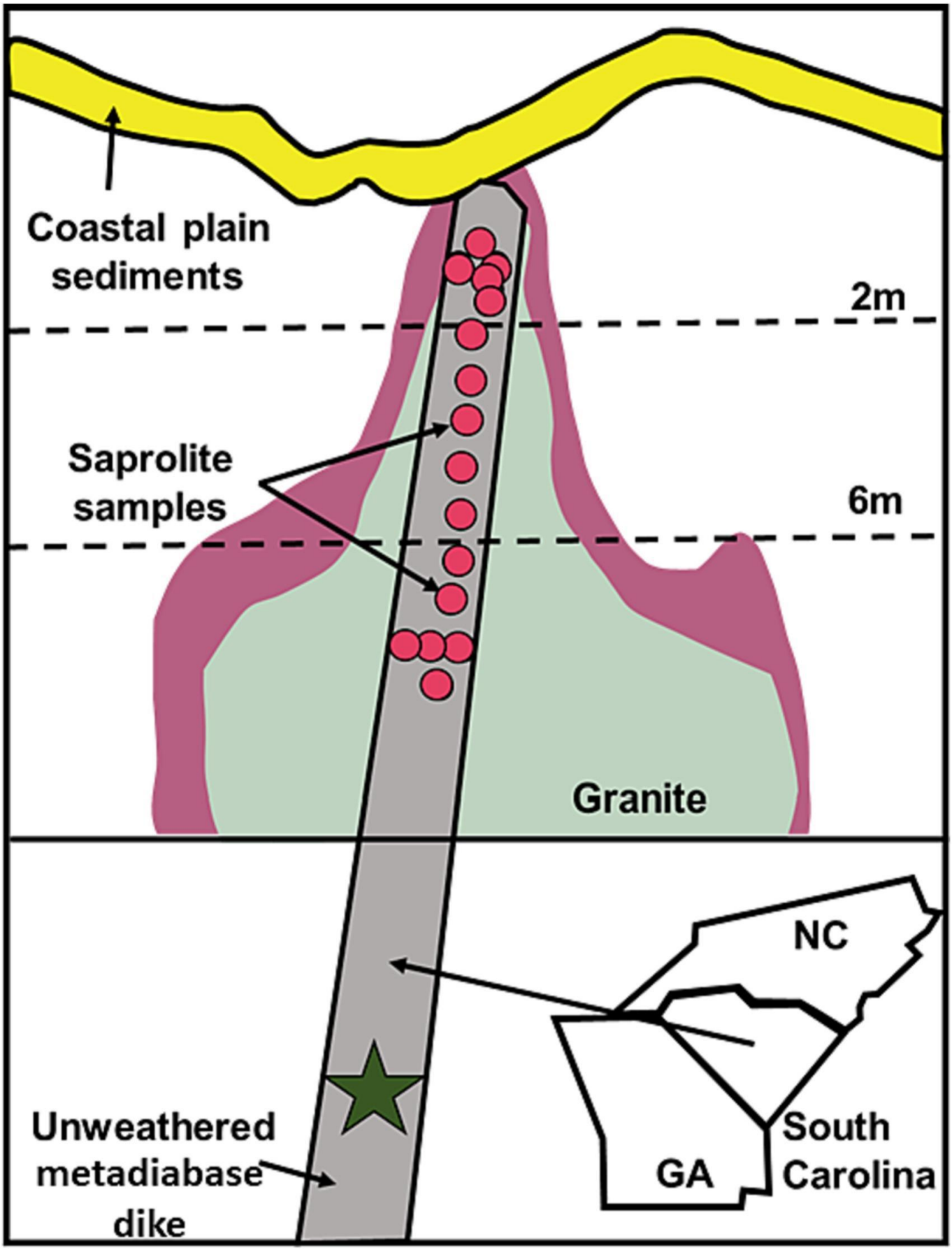
Coastal plain sediments
2m
Saprolite samples
6m
Granite
NC
Unweathered metadiabase dike
South Carolina
GA

Figure 1

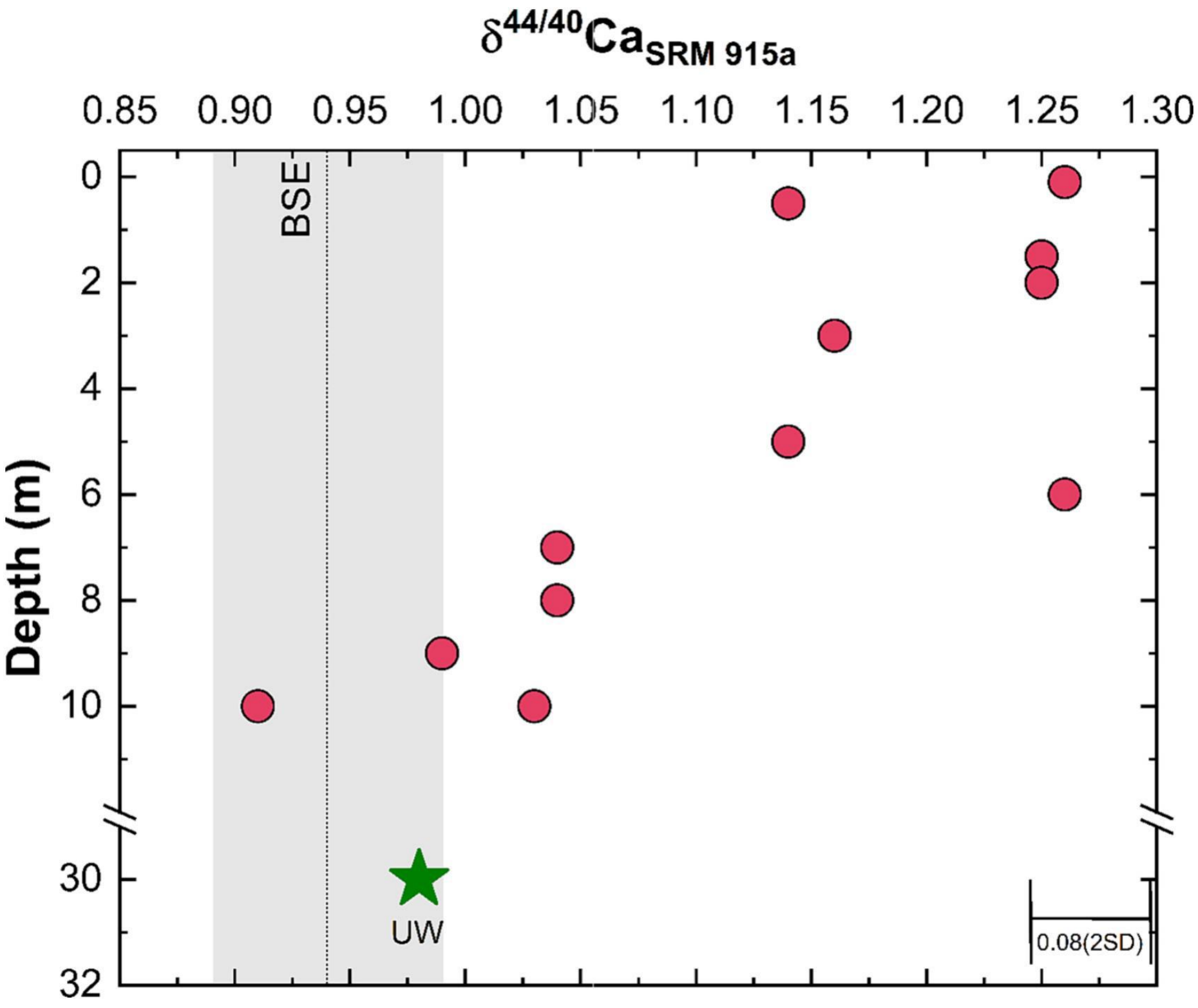
$\delta^{44/40}Ca_{SRM\ 915a}$
0.85
0.90
0.95
1.00
1.05
1.10
1.15
1.20
1.25
1.30
Depth (m)
0
2
4
6
8
10
30
32
BSE
UW
0.08(2SD)

Figure 2

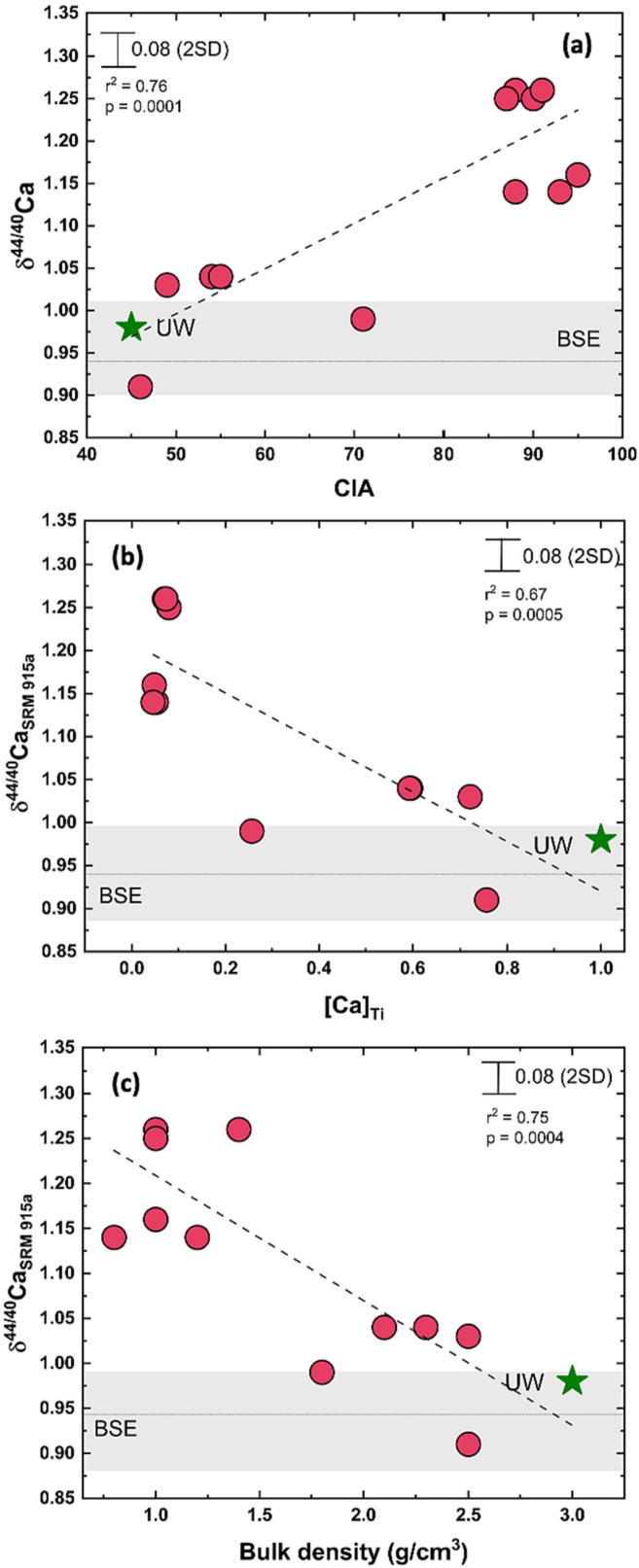
(a)
0.08 (2SD)
r² = 0.76
p = 0.0001
UW
BSE
δ44/40Ca
CIA
(b)
0.08 (2SD)
r² = 0.67
p = 0.0005
UW
BSE
δ44/40CaSRM 915a
[Ca]Ti
(c)
0.08 (2SD)
r² = 0.75
p = 0.0004
UW
BSE
δ44/40CaSRM 915a
Bulk density (g/cm3)

Figure 3

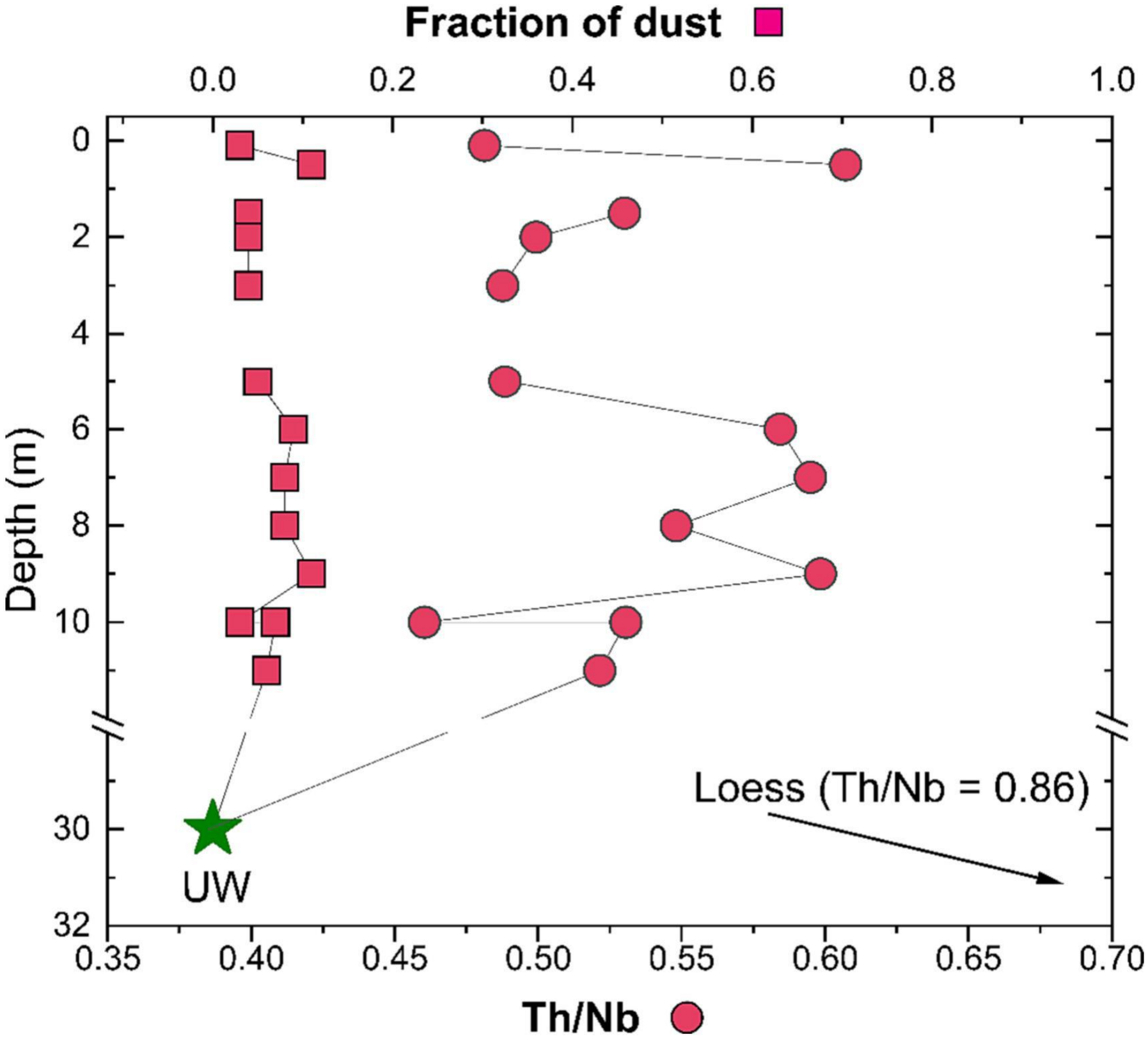
Fraction of dust
0.0
0.2
0.4
0.6
0.8
1.0
Depth (m)
0
2
4
6
8
10
30
32
UW
Loess (Th/Nb = 0.86)
0.35
0.40
0.45
0.50
0.55
0.60
0.65
0.70
Th/Nb

Figure 4

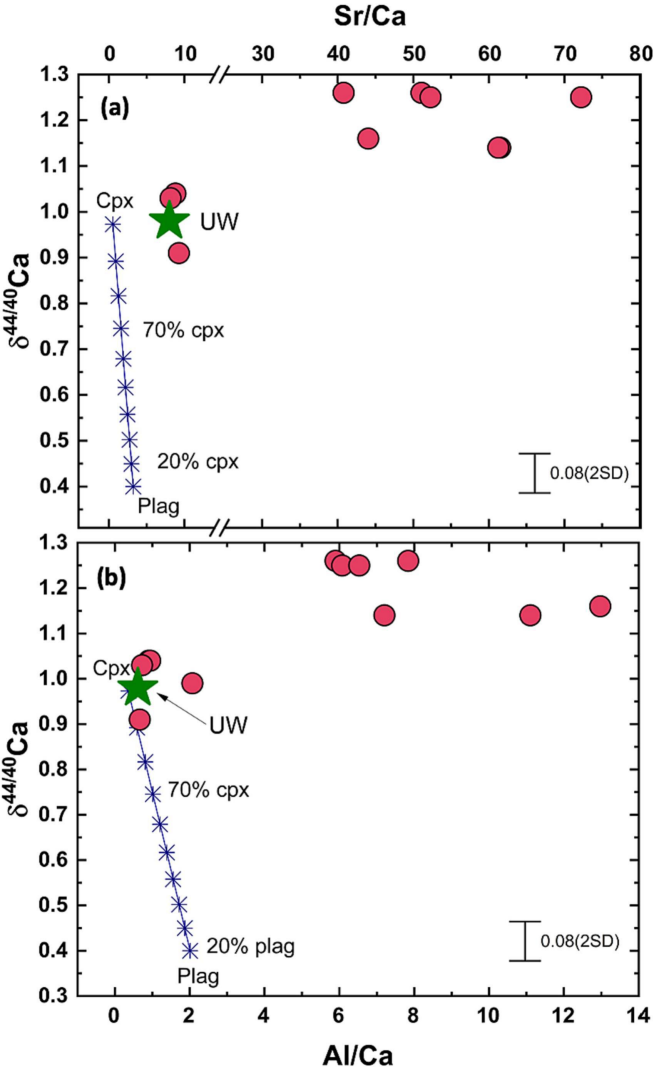
Sr/Ca
0
10
30
40
50
60
70
80
(a)
Cpx
UW
70% cpx
20% cpx
Plag
0.08(2SD)
δ44/40Ca
1.3
1.2
1.1
1.0
0.9
0.8
0.7
0.6
0.5
0.4
(b)
Cpx
UW
70% cpx
20% plag
Plag
0.08(2SD)
0.3
0
2
4
6
8
10
12
14
Al/Ca

Figure 5

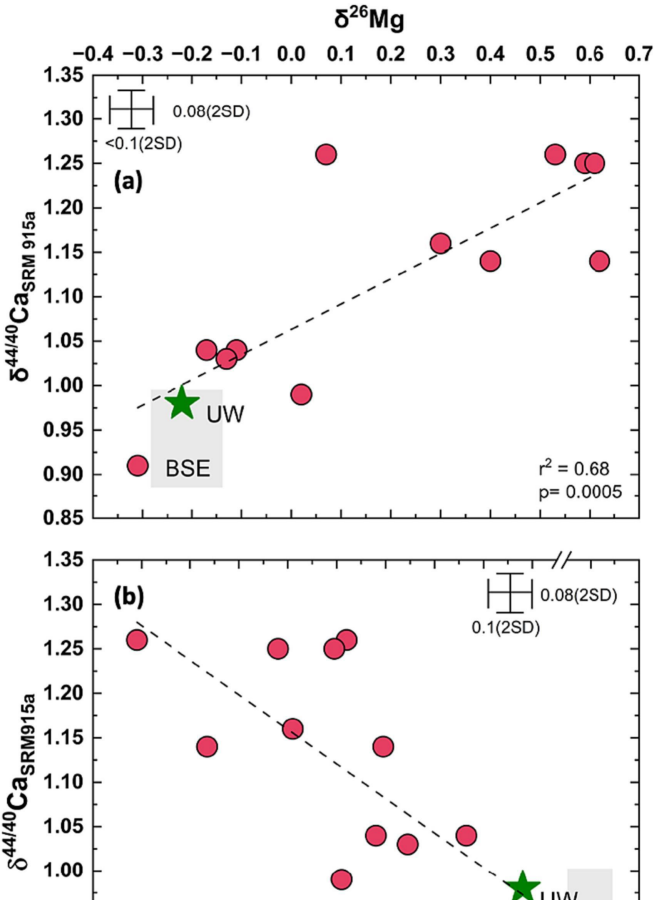
δ26Mg
−0.4 −0.3 −0.2 −0.1 0.0 0.1 0.2 0.3 0.4 0.5 0.6 0.7
0.08(2SD)
<0.1(2SD)
(a)
δ44/40CaSRM 915a
UW
BSE
r2 = 0.68
p= 0.0005
(b)
0.08(2SD)
0.1(2SD)
δ44/40CaSRM915a
UW
BSE
r2 = 0.48
p= 0.009
−22 −20 −18 −16 −14 −12 −10 −8 −6 −4 4 6
δ7Li

Figure 6

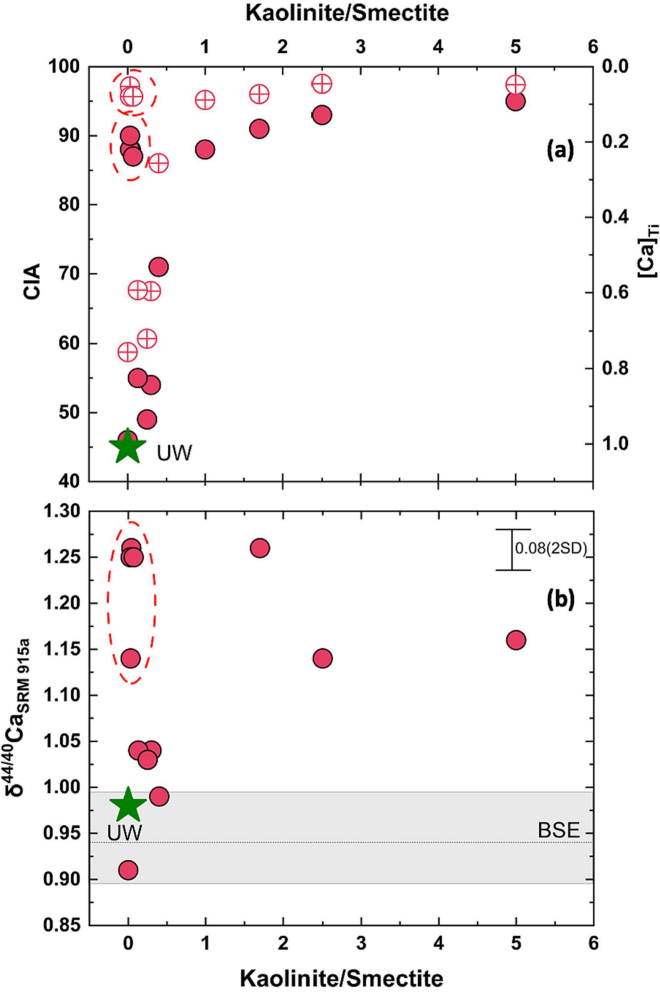
Kaolinite/Smectite
0
1
2
3
4
5
6
100
90
80
70
60
50
40
CIA
0.0
0.2
0.4
0.6
0.8
1.0
[Ca]Ti
(a)
UW
1.30
1.25
1.20
1.10
1.05
1.00
0.95
0.90
0.85
δ44/40CaSRM 915a
0.08(2SD)
(b)
UW
BSE
Kaolinite/Smectite

Figure 7